

# Impact of 3-Cyanopropionic Acid Methyl Ester on the Electrochemical Performance of $\text{ZnMn}_2\text{O}_4$ as Negative Electrode for Li-Ion Batteries

Zijian Zhao, Lydia Gehrlein, Annika Bothe, Julia Maibach, Andrea Balducci, and Sonia Dsoke\*

Due to their high theoretical capacity, transition metal oxide compounds are promising electrode materials for lithium-ion batteries. However, one drawback is associated with relevant capacity fluctuations during cycling, widely observed in the literature. Such strong capacity variation can result in practical problems when positive and negative electrode materials have to be matched in a full cell. Herein, the study of  $\text{ZnMn}_2\text{O}_4$  (ZMO) in a nonconventional electrolyte based on 3-cyanopropionic acid methyl ester (CPAME) solvent and  $\text{LiPF}_6$  salt is reported for the first time. Although ZMO in  $\text{LiPF}_6$ /CPAME electrolyte displays a dramatic capacity decay during the first cycles, it shows promising cycling ability and a suppressed capacity fluctuation when vinylene carbonate (VC) is used as an additive to the CPAME-based electrolyte. To understand the nature of the solid electrolyte interphase (SEI), the electrochemical study is correlated to *ex situ* X-ray photoelectron spectroscopy (XPS).

## 1. Introduction

Conversion/alloying-type metal oxide (or sulfide) materials are gaining increasing attention as a new class of negative electrodes for Li-ion batteries (LIBs). Compared with the electrodes based on only conversion or only alloying mechanisms, in this type of compound, lithium storage relies on the combination of both mechanisms, which can confer much higher theoretical capacities, lower average operational potentials, and smaller discharge/charge voltage hysteresis.<sup>[1]</sup> After the conversion reaction, metallic nanograins are generated and dispersed in the  $\text{Li}_2\text{O}$  (or  $\text{Li}_2\text{S}$ ) matrix, which buffers the volume change during the subsequent alloying process. Among different possible metals, which can form an alloy

with lithium, zinc has some advantages over other metals in terms of its high availability, low toxicity, and relatively small volume variation upon alloying/dealloying.<sup>[2,3]</sup> As representative of conversion/alloying type materials,  $\text{ZnTM}_2\text{O}_4$  (with  $\text{TM} = \text{Fe}, \text{Co}, \text{Mn}$ ) spinel-type compounds exhibit promising perspectives for LIB applications.<sup>[4]</sup> The use of Mn and Fe addresses sustainability issues due to the higher abundance of these metals over Co in the Earth crust. However, these materials still need to be optimized to overcome their intrinsic issues.


The issues that need to be addressed are the low electronic conductivity, the considerable amount of solid electrolyte interphase (SEI) formation, the large irreversible capacity at the first cycle and the large voltage hysteresis upon charge and discharge.<sup>[1,3]</sup> The elucidation of the electrochemical storage mechanism and the understanding of the SEI composition are essential to finding solutions for these challenges. The  $\text{Li}^+$  storage in  $\text{ZnMn}_2\text{O}_4$  (ZMO) relies on the redox (conversion-type) mechanism followed by the alloying process, which induces the reversible storage of 7  $\text{Li}^+$  pfu ( $784 \text{ mAh g}^{-1}$ ).<sup>[5,6]</sup> During the first lithiation, the spinel ZMO converts to Li–Zn alloy and metallic Mn nanoparticles embedded in amorphous  $\text{Li}_2\text{O}$ . During the subsequent delithiation, these products convert to MnO and ZnO.<sup>[6]</sup> Carbon-coating is proved to be an effective method to improve the cycling stability of the electrode. The coated layer can suppress the pulverization of the active material and can inhibit excessive SEI growth.<sup>[7]</sup> The SEI growth is also viewed from a positive perspective in the scientific community:

Dr. Z. Zhao, L. Gehrlein, Dr. J. Maibach, Dr. S. Dsoke  
Institute for Applied Materials (IAM)  
Karlsruhe Institute of Technology (KIT)  
Hermann-von-Helmholtz-Platz 1, 76344 Eggenstein-Leopoldshafen,  
Germany  
E-mail: sonia.dsoke@kit.edu

Dr. Z. Zhao  
College of Chemical Engineering and Material Science  
Tianjin University of Science & Technology (TUST)  
Tianjin 300457, China

A. Bothe, Prof. A. Balducci  
Institute for Technical Chemistry and Environmental Chemistry  
Friedrich-Schiller-University Jena  
07743 Jena, Germany

Dr. S. Dsoke  
Helmholtz-Institute Ulm for Electrochemical Energy Storage (HIU)  
Karlsruhe Institute of Technology (KIT)  
3640 Karlsruhe, Germany

 The ORCID identification number(s) for the author(s) of this article can be found under <https://doi.org/10.1002/ente.202100247>.

© 2021 The Authors. Energy Technology published by Wiley-VCH GmbH. This is an open access article under the terms of the Creative Commons Attribution License, which permits use, distribution and reproduction in any medium, provided the original work is properly cited.

DOI: 10.1002/ente.202100247

several authors reported that the SEI could be responsible for extra charge storage in conversion-type materials.<sup>[8]</sup> However, for practical applications, the extra capacity can be viewed as a positive feature only when it is reached in a relatively short number of cycles (i.e., like formation cycles) and then it remains constant upon long-term cycling. In our previous study, we observed a constant capacity increase in ZMO electrode, followed by a decrease.<sup>[6]</sup> This fluctuation is not beneficial in a full cell system where the capacities of positive and negative electrodes have to be carefully balanced. In this context, the choice of the electrolyte may play a crucial role.

Carbonate-containing electrolytes used in commercial LIBs are mainly formulated by dissolving lithium hexafluorophosphate, 1 M LiPF<sub>6</sub>, in cyclic carbonates like ethylene carbonate (EC) and linear carbonates such as dimethyl carbonate (DMC). Based on its relatively low cost and superior properties (such as ionic conductivity, chemical stability to electrodes, and current collectors), LiPF<sub>6</sub> dissolved in a mixture of carbonates (e.g., LP30 commercial electrolyte) is considered as the most sustainable electrolyte for LIBs for more than two decades.<sup>[9,10]</sup> LP30 forms a stable, protective SEI on typical negative electrodes, such as graphite, and it is, therefore, the best choice for such kind of materials.<sup>[11]</sup> However, moving to other types of electrode materials does not imply that the “standard” electrolyte will still be the best option. A paradigm change is necessary to match electrolytes to new materials. Moreover, other aspects have to be taken into account when considering the commercial LP30 electrolyte. LiPF<sub>6</sub> in EC/DMC is thermally unstable and can decompose into LiF and PF<sub>5</sub>. Furthermore, PF<sub>5</sub> can be hydrolyzed in the presence of residual water to form HF and PF<sub>3</sub>.<sup>[12]</sup> The anodic stability of the conventional LP30 electrolyte is also limited to 4.3 V.<sup>[13,14]</sup> Exploring safer organic solvents able to dissolve LiPF<sub>6</sub> and able to operate over a wide temperature range and in an extended electrochemical stability window has received increasing attention.<sup>[10,14]</sup> Recently, 3-cyanopropionic acid methyl ester (CPAME), has been proposed as an alternative electrolyte for LIBs, electrochemical capacitors, and lithium-ion capacitors.<sup>[15–17]</sup> The results of these studies show that CPAME-based electrolytes display a promising set of transport and thermal properties and that their use allows the realization of devices with high and stable performance.

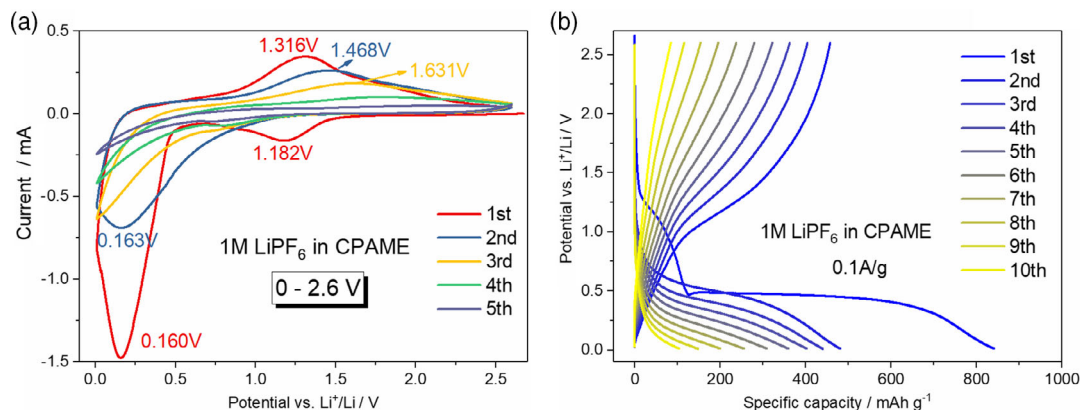
At 30 °C, the electrolyte 1 M LiPF<sub>6</sub> in CPAME displays a conductivity of 3 mS cm<sup>-1</sup>, a viscosity of 10 mPa s, and an overall electrochemical stability exceeding 5.5 V (at room temperature). Furthermore, it is stable up to 100 °C.<sup>[15]</sup>

In this study, we investigated the use of a CAPME-based electrolyte in combination with ZMO -based electrodes. To the best of our knowledge, these innovative electrolytes have not been used with conversion/alloying-type materials before. The main goal of this study is to understand the impact of CAPME-based electrolytes on the cycling stability of ZMO. As mentioned earlier, these electrodes are characterized by a rather strong capacity fluctuation over cycling in conventional electrolytes. This fluctuation represents a limitation for the use of ZMO-based electrodes in practical systems; therefore, its suppression is essential for the development of LIB based on this high-capacity anodic material.

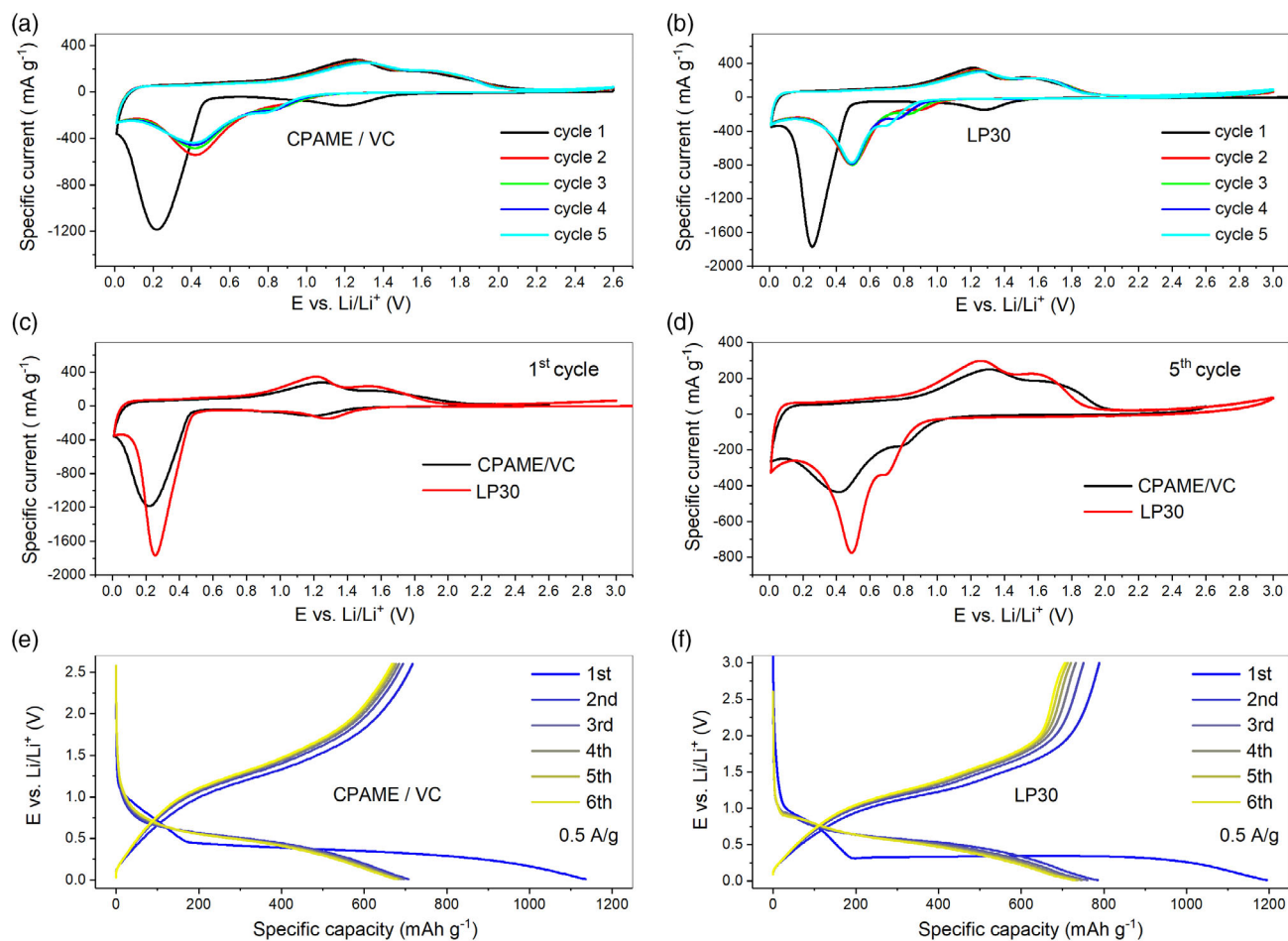
## 2. Results and Discussion

Figure 1 shows the CV and galvanostatic cycle profiles of ZMO electrodes in 1 M LiPF<sub>6</sub>/CPAME electrolyte. As a first attempt, the upper potential cut-off was set to 3 V versus Li<sup>+</sup>/Li, as usually done with this material and a standard LP30 electrolyte.<sup>[6]</sup> However, an increase in oxidative current is observed at potentials higher than 2.6 V versus Li<sup>+</sup>/Li, which leads to a very fast capacity decay (Figure S1, Supporting Information). To avoid this parasitic reaction, in the following experiments, the upper potential cut-off was limited to 2.6 V. However, it is evident that the fast fading of the capacity is not due to the choice of the potential cut-off, as the shape of the CV curves continuously changes with every cycle also in the restricted potential span (Figure 1a). After only three cycles, the characteristic redox peaks cannot be distinguished anymore. The poor stability is confirmed by galvanostatic cycling, as shown in Figure 1b: after only 10 cycles, the capacity drops from 480 to 100 mAh g<sup>-1</sup>.

CPAME is known as a nonfilm-forming solvent and the proper formation of a protective passivation film seems to be essential for the cyclability of ZMO. To form a protective film, 2 wt% VC was added to the CPAME-based electrolyte (CPAME/VC). In the presence of the VC additive, after the first cycle, the CV profiles



**Figure 1.** a) CV at 0.1 mV s<sup>-1</sup> on ZMO electrodes with 1 M LiPF<sub>6</sub>/CPAME electrolyte in the potential range 0–2.6 V. b) Galvanostatic profiles of a ZMO electrode recorded at 0.1 A g<sup>-1</sup> in the potential range 0–2.6 V.



**Figure 2.** Consecutive CV curves recorded at a scan rate of  $0.1 \text{ mV s}^{-1}$  on ZMO electrodes in a) CPAME/VC and b) LP30; comparison of the c) first CV and d) fifth CV in the two electrolytes; galvanostatic potential profiles at a current density of  $0.5 \text{ A g}^{-1}$  of ZMO electrodes in e) CPAME/VC and f) LP30.

are overlapping, indicating improved stability (Figure 2a). The electrochemical signature is similar to the one achieved with the commercial electrolyte LP30, with some small differences in current intensity and peaks broadening (Figure 2a–d).

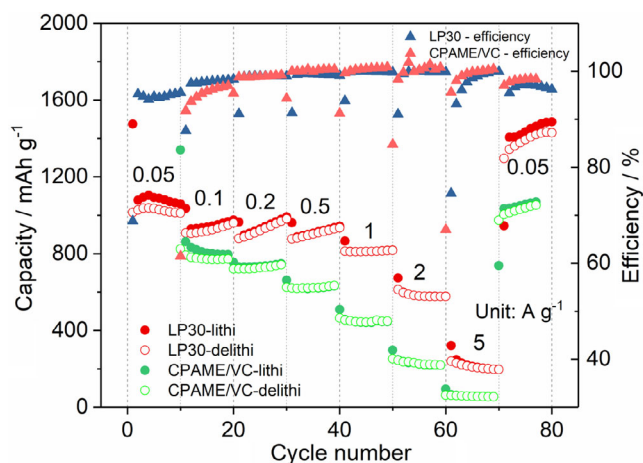
After the first cycle, the voltammograms show two cathodic (at about 0.8 and 0.5 V vs  $\text{Li}^+/\text{Li}$ ) and two anodic peaks (at about 1.3 and 1.7 V vs  $\text{Li}^+/\text{Li}$ ), respectively, correlated to the steps of reduction and oxidation of  $\text{ZnO-MnO}$  material.

Figure 2d shows the direct comparison of the fifth cycle of ZMO electrodes in the two electrolytes. The redox peaks in LP30 are sharper and less polarized due to the different conductivity and viscosity of the electrolytes.<sup>[15]</sup> The galvanostatic profiles recorded at  $0.5 \text{ A g}^{-1}$  are shown in Figure 2e,f. Apart from a slightly lower capacity, the electrode with CPAME/VC performs similarly to the one with the commercial electrolyte. The presence of a small amount of VC in the CPAME system can drastically improve the performance by forming a passivation layer on the surface of ZMO.

In CPAME/VC electrolyte, the rate capability of ZMO is poorer than in LP30 (Figure 3), which can be correlated to the higher viscosity and lower conductivity of this electrolyte. However, while at each current density, an increase in capacity can be observed in LP30, in CPAME/VC the capacity values are

more stable. This result indicates higher stability of ZMO in the CPAME/VC electrolyte than in the LP30, where severe capacity fluctuations during cycling can be observed.<sup>[6]</sup>

Indeed, during cycling, the capacity of the cell with CPAME/VC decreases slowly and continuously. In contrast, ZMO undergoes dramatic capacity fluctuations in LP30 (Figure 4a). In LP30, the capacity slightly decreases during the initial  $\approx 30$  cycles, then increases dramatically during 30–100 cycles and finally decreases again (100–150 cycles). Interestingly, the capacities become nearly identical after 150 cycles in both electrolytes. To understand if there are any relevant effects due to the presence of VC, an electrode was cycled in LP30 electrolyte with the addition of the same amount of VC (LP30/VC). Also in this case, drastic capacity variations are observed, even stronger than with the pure LP30, indicating the critical role of the carbonate-type component on the contribution to the extracapacity. As mentioned in Section 1, such strong capacity fluctuations are detrimental for a real-world battery, where capacities of positive and negative electrodes should be matched as precisely as possible. Indeed, a strong mismatch in capacity during cycling might result in battery failure. As shown, ZMO, in combination with CPAME/VC, does not undergo these undesirable capacity fluctuations, which is an advantage from a practical point of view. In addition, the



**Figure 3.** Rate test with current densities from 0.1 to 5.0 A g<sup>-1</sup> on ZMO electrodes in CPAME/VC and LP30 electrolytes.

CPAME-VC-based electrolyte confers the best Coulombic efficiency over the three electrolytes (Figure 4b), which approaches after the initial cycles ≈100%. This result outlines that beyond the choice of the active material, the electrolyte plays a vital role on mitigating side reactions and on the cycling life of a cell.

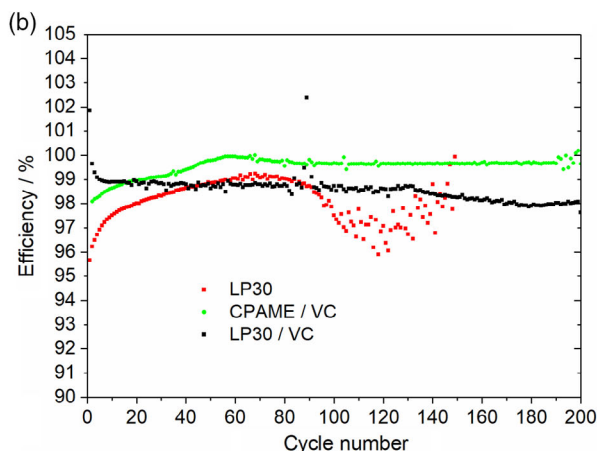
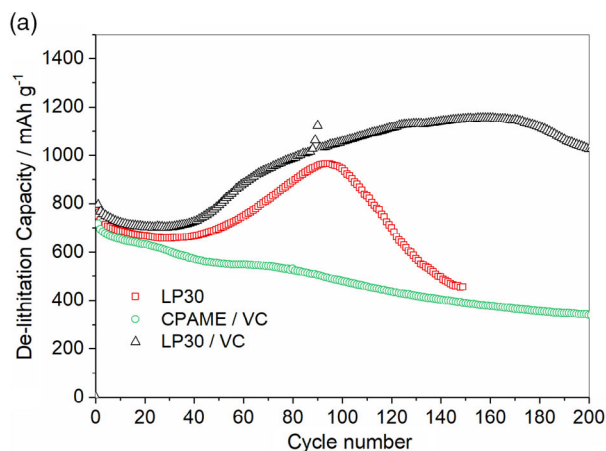


**Figure 4.** Long-term cycling test at 0.5 A g<sup>-1</sup> on ZMO electrodes in LP30, CPAME/VC, and LP30/VC electrolytes; a) evolution of capacity versus cycle number. b) Corresponding Coulombic efficiency.

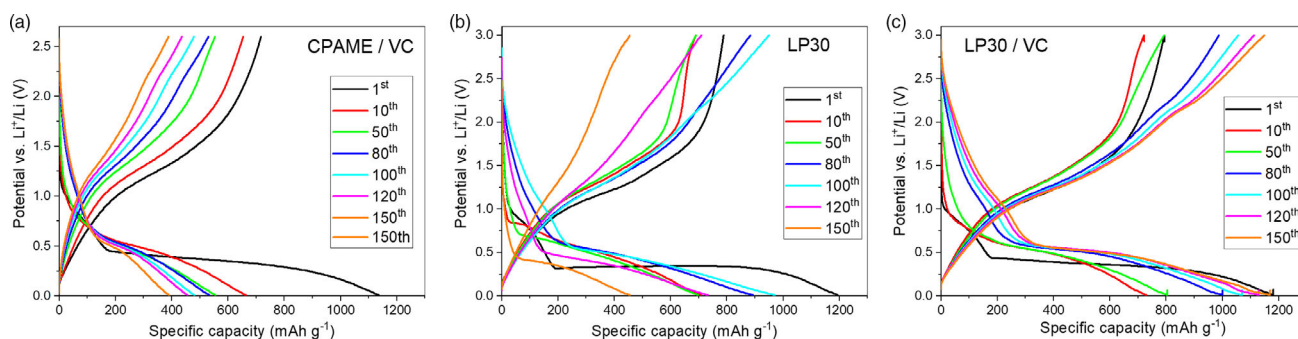


**Figure 5.** Potential profiles upon cycling of the ZMO electrode with the a) CPAME/VC, b) LP30, and c) LP30/VC electrolytes.

**Figure 5** shows the evolution of the potential profiles in the three electrolytes. In all cases, the curves progressively change to a pseudocapacitive-linear feature as the initially sloped plateau is progressively smoothed in the high potential region. In the case of LP30, the capacity increases and reaches its maximum after about 100 cycles (light blue curve in Figure 5b). In the case of CPAME/VC, the shape of the curve at the 100th cycle is similar to the ones obtained in LP30 and LP30/VC but with a lower capacity (Figure 5a).

To obtain information about electrolyte decomposition products, the XPS technique was used. The analyzed electrodes were cycled in the following electrolytes: pure CPAME, CPAME/VC, pure LP30, and LP30/VC. The analyses were carried out on samples after the 5th and the 200th cycles. All spectra were measured on electrodes at delithiated states (i.e., after conditioning at 3 V vs Li<sup>+</sup>/Li for 1 h) and all peaks were assigned according to literature.<sup>[18]</sup> **Figure 6** shows the C 1s and N 1s spectra of electrode cycled in pure CPAME and CPAME/VC, as well as the C 1s spectra of LP30 and LP30/VC. O 1s and F 1s spectra can be found in Figure S1 and S2, Supporting Information.

Figure 6a shows the C 1s photoelectron spectra of electrodes cycled in pure CPAME and CPAME/VC. The spectrum of the CPAME-cycled electrode shows six peaks. The peak at 284.4 eV corresponds to sp<sup>2</sup>-hybridized carbon in carbon black and in the SBR-binder. This peak was fitted asymmetrically



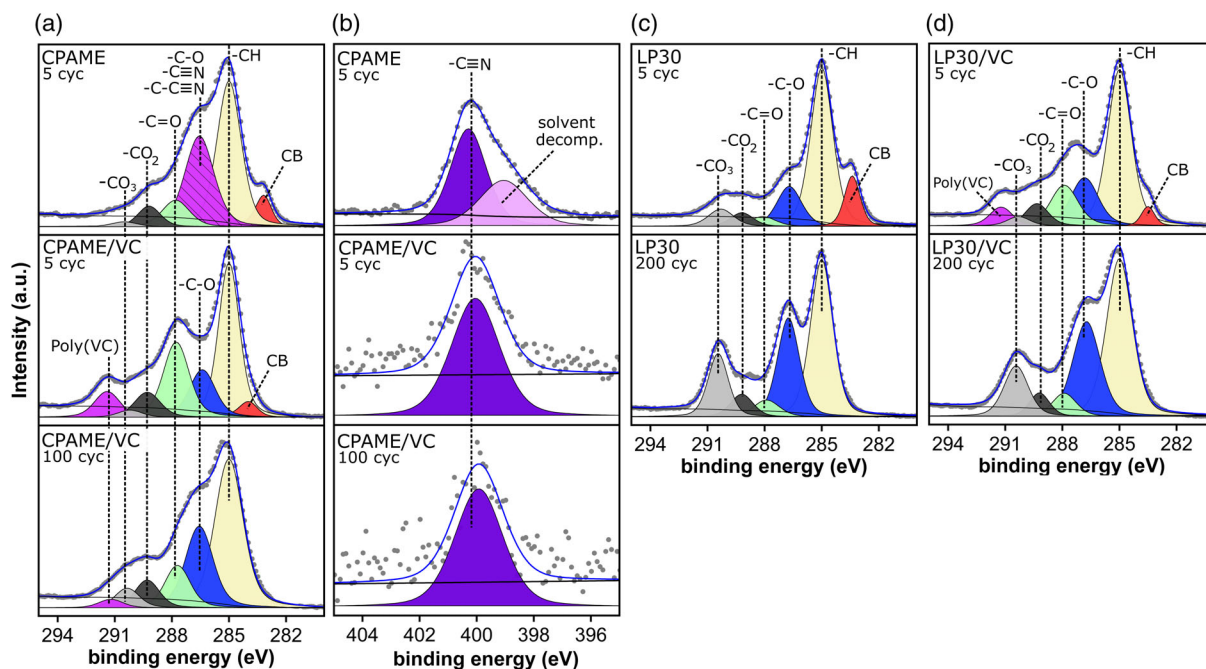


**Figure 6.** a) C 1s spectra of CPAME, CPAME/VC-5 cyc, and CPAME/VC-200 cyc, b) N 1s of CPAME, CPAME/VC-5 cyc, and CPAME/VC-200 cyc, and c) C 1s spectra of LP30-5 cyc and LP30-200 cyc, and d) C 1s spectra of LP30/VC-5 cyc and LP30/VC-200 cyc.

due to  $sp^2$ -hybridized carbon. The second peak at 285 eV corresponds to hydrocarbons contained in the SEI.  $-C-O$  compounds as well as nitrile groups ( $-C\equiv N$  and  $C-C\equiv N$ ) of the CPAME solvent give rise to a peak at around 286.6 eV. All the three components were fitted as one because their binding energies are very close to each other. The peaks at 288.2, 289.1, and 290.8 eV are resulting from  $-C=O$ ,  $-CO_2$ , and  $-CO_3$  components, respectively, which are part of the SEI. Peaks corresponding to the sodium carboxymethyl-cellulose (Na-CMC) binder overlap with the  $-C-O$  (286.6 eV) and  $-CO_2$  (289.1 eV) peaks of the SEI.

The N 1s spectra of the electrode with pure CPAME and CPAME/VC are shown in Figure 6b. In pure CPAME, two peaks are observed after five cycles. The first peak at 400 eV corresponds to the nitrile group ( $-C\equiv N$ ) deriving from CPAME residues and CPAME decomposition products. A second decomposition product is observed at around 399 eV. It represents compounds with higher electronic density on the nitrogen atom (e.g.,  $C=N^-$  groups).<sup>[19]</sup> The high content of these two nitrogen-containing compounds indicates a large amount of CPAME solvent being decomposed during cycling. This resulting interfacial film can explain the poor electrochemical performance of pure CPAME. This film probably possesses low lithium-ion conductivity and may also break apart the conductive network among carbon black,  $ZnMnO_4$ , ZnO, and MnO, creating electrically insulated regions.

The first difference observed when adding VC to CPAME is the decrease in the intensity of the peaks related to the N-containing decomposition products. This decrease can be observed in the C 1s spectrum at around 286.6 eV (Figure 6a). Compared with the spectrum related to the system without VC, this peak now mainly consists of  $-C-O$ -type compounds. For the N 1s spectrum, only the peak associated with nitriles

at 400 eV remains and no second peak is observable (Figure 6b). The overall nitrogen concentration in the SEI decreases from 4.7 at% (without VC) to 1.0 at% (with VC), as shown in Table 1. The second difference is the emergence of VC decomposition products such as poly(VC) observed in the C 1s spectrum at around 291.3 eV ( $-CO_{3,poly(VC)}$ ) and 288.2 eV ( $C-CO_{3,poly(VC)}$ ).<sup>[20]</sup>

Comparing the spectra of CPAME/VC, LP30/VC, and LP30, similar SEI chemical compositions are observed (Figure 6a,c, d). After five cycles, the intensity related to the carbon black peak at 283.5 eV is higher for the LP30-sample. In the presence of VC (i.e., LP30/VC & CPAME/VC), the peak related to the carbon black peak is less intense, suggesting a thicker SEI. This observation is contrary to findings in the literature, where VC is found to generate a thinner SEI when using graphite electrodes.<sup>[21]</sup> After 200 cycles, the main difference lies in the intensity of the carbonate peak at 290.8 eV. The electrodes cycled in LP30 and LP30/VC demonstrate higher  $-CO_3$  abundance in the SEI than the electrode cycled in CPAME/VC. This could be explained by the formation of a less stable SEI in the case of LP30 and LP30/VC, leading to higher electrolyte consumption and carbonate formation.

However, the higher carbonate content is not a conclusive explanation for the higher capacities of the electrodes cycled in LP30 and LP30/VC. In fact, overall, the SEI compositions of electrodes cycled in LP30, LP30/VC, and CPAME/VC are very similar. This is not surprising as the SEI is being formed, in all cases, out of the decomposition of carbonate-containing compounds (i.e., VC or EC & DMC). Therefore, it is difficult to determine whether and how the SEI composition influences the difference in capacity fluctuation. Overall, CPAME/VC seems to be a good electrolyte system, forming a stable and protective

**Table 1.** Atomic percentages (at%) calculated from XPS.

	Species	CPAME	CPAME/VC	CPAME/VC	LP30/VC	LP30/VC	LP30	LP30
		5cyc	5cyc	200cyc	5cyc	200cyc	5cyc	200cyc
C 1s	CB	4.4	1.7	0	1.7	0	6.5	0
	CH <sub>2</sub>	19.5	15.1	19.9	24.9	17.3	29.2	16.9
	—C—O	12.4	5.7	10.7	9.0	9.9	8.2	10.6
	C=O	4.5	9.0	5.1	7.6	2.3	2.1	2.1
	—CO <sub>2</sub>	2.0	3.0	3.2	3.5	1.5	2.8	2.5
	—CO <sub>3</sub>	0.9	0.8	2.3	1.4	5.3	3.6	6.2
	Poly(VC)	0	3.0	1.0	2.9	0	0	0
N 1s	—C≡N	1.8	1.0	0.5	0	0	0	0
	Solv. decomp.	2.9	0	0	0	0	0	0
O 1s	Li <sub>2</sub> O	0	0	1.6	0	0.8	0	0
	ROLi	1.3	0	6.8	0	6.8	3.1	2.3
	—C=O	13.6	8.3	11.2	15.2	15.5	17.3	20.7
	—C—O, Li <sub>x</sub> PF <sub>y</sub> O <sub>z</sub>	3.5	7.1	2.2	8.3	4.8	6.5	9.6
	Poly(VC)	0	7.4	1.5	7.4	0	0	0
F 1s	Li <sub>x</sub> PF <sub>y</sub>	7.4	15.8	2.4	4.5	3.9	3.6	7.4
	LiF	5.0	1.1	0.7	0.6	2	1.7	0.6
P 2p	Li <sub>x</sub> PF <sub>y</sub> O <sub>z</sub>	0.6	0.6	0.2	0.2	0.2	0.2	0.1
	Li <sub>x</sub> PF <sub>y</sub>	1.0	1.3	0.3	0.7	0.7	0.7	1.2
Li 1s	Li—X	17.9	14.0	31.0	12.0	28.9	14.7	19.4

SEI layer on ZMO electrodes. A quantitative estimation of the SEI thickness is not possible from XPS due to the fact that the active material under the passivation layer cannot be detected. However, while LP30 and LP30/VC show an increase in carbonates during cycling, no additional decomposition products deriving from the CPAME solvent are observed for the CPAME/VC electrolyte after 200 cycles. The increase in carbonate content in the case of LP30 and LP30/VC can be correlated to an unstable SEI and continuous electrolyte decomposition, leading to the extra capacity. On the other side, the addition of a small amount of VC in CPAME prevents excessive solvent decomposition, hence positively influencing the cycling behavior and suppressing the capacity fluctuation. Table 1 shows the atomic percentages as calculated from XPS. The percentage of detected Li increases with the cycle number for all electrolytes. As the electrodes are analyzed in their delithiated state (where Li<sub>2</sub>O should not be present, or present in a very small amount), the presence of Li can be attributed to the decomposition of the salt on the electrode surface. However, as shown in Table 1 and in the O1s spectra in Figure S2, Supporting Information, Li<sub>2</sub>O is detected on electrodes cycled in CPAME/VC and LP30/VC after 200 cycles. This could be correlated to a partial irreversible reaction, leading to residual Li<sub>2</sub>O on the surface.

### 3. Conclusions

This work reports for the first time about the electrochemical behavior of CPAME-based electrolytes with conversion-type materials (i.e., ZMO, in this specific case). CPAME alone

strongly decomposes on the electrode, without forming a proper protective and Li-conductive layer, resulting in a dramatic drop of capacity during the initial cycles. It is found here that the presence of a minimum amount of carbonate (in this case VC) is vital to suppress the excessive CPAME decomposition. The combination of CPAME and VC leads to stable cycling performance of ZMO without capacity variations and improved reversibility. On the contrary, in agreement with the literature, carbonate-based electrolytes such as LiPF<sub>6</sub> in EC/DMC lead to continuous decomposition and associated strong capacity variations during cycling. XPS analysis carried out on relatively fresh electrodes (after 5 cycles) and on “aged” electrodes (after 200 cycles), reveals an increase in the amount of carbonates when the electrodes are cycled in EC/DMC and EC/DMC/VC-based electrolytes. On the other side, no such increase is observed for the CPAME/VC-solvent mixture. Although the electrolyte composition based on CPAME can be further improved to obtain even better capacity retention over time, this study opens up a new possibility of combinations of conversion/alloy-type materials with alternative solvents, which can suppress the dramatic capacity variation.

### 4. Experimental Section

*Synthesis of the ZMO Nanoparticles:* Based on our previous report,<sup>[6]</sup> the ZMO nanoparticles were prepared via the oxalic acid coprecipitation method. Zinc acetate dihydrate (Zn(CH<sub>3</sub>COO)<sub>2</sub>·2H<sub>2</sub>O, Alfa Aesar, 98%), manganese acetate tetrahydrate (Mn(CH<sub>3</sub>COO)<sub>2</sub>·4H<sub>2</sub>O, Aldrich, 99%), and oxalic acid (H<sub>2</sub>C<sub>2</sub>O<sub>4</sub>, Aldrich, 99%) were used without further purification. Zinc acetate dihydrate and manganese acetate tetrahydrate were dissolved in deionized water to form a 0.4 M solution. This zinc

acetate and manganese acetate (Mn/Zn = 2:1 molar ratio) solution was then added into 0.4 M oxalic acid aqueous solution (oxalic acid/metal ions = 1.5:1 molar ratio) and stirred at 600 rpm for 0.5 h. The obtained precipitate was washed and centrifuged several times with deionized water and ethanol. The precursor was obtained after drying at 80 °C for 12 h. Subsequently, the cp-ZMO was calcined at 500 °C for 3 h in air, labeled as ZMO.

**Preparation of the Electrolytes:** The electrolytes based on 1 mol L<sup>-1</sup> of LiPF<sub>6</sub> salt dissolved in 3-cyanopropionic acid methyl ester pure (CPAME) and with 2% VC additive (CPAME/VC) were prepared under a dry atmosphere in a glovebox. LP30 electrolyte (1 M LiPF<sub>6</sub> in EC/DMC = 1:1 by mass ratio) was purchased from BASF. A fourth electrolyte was prepared by adding 2% VC as the additive (LP30/VC). All electrolytes were stored and used in a glovebox. The conductivity, viscosity, thermal, and electrochemical stabilities of the electrolyte are available in previous studies.<sup>[15,17]</sup>

**Electrodes Preparation and Cells Assembly:** The working electrodes were prepared by mixing ZMO (60 wt%), carboxymethyl cellulose-styrene-butadiene rubber (CMC-SBR) binder (20 wt%, R6020/1001, Solvay), and carbon black (20 wt%) in water. The slurry was coated on a copper foil. The coated foils were dried at 80 °C for 12 h in a vacuum oven. Afterward, the foils were punched out into disc electrodes (φ 12 mm) with active mass loading of 1.2–1.6 mg cm<sup>-2</sup>. The assembled coin cells (CR2032 type) consist each of a working electrode, a Whatman glass-fiber separator (φ 17 mm), a lithium foil (φ 15 mm, Alfa Aesar) as counter electrode, and 180 μL of electrolyte. The coin cells were assembled in an argon-filled glovebox (MB200, MBraun GmbH) and kept in a climate chamber (Binder) at 25 °C during the electrochemical tests. Galvanostatic charge/discharge (GCD) and cyclic voltammetry (CV) were carried out using a Bio-Logic potentiostat equipped with EC-Lab software for data analysis.

**Characterization of the Electrode Materials via XPS:** XPS measurements were carried out with a K $\alpha$  spectrometer from Thermo-Fisher Scientific. A microfocused, monochromated Al K $\alpha$  X-ray source with 400 μm spot size was applied. The pass energy was set to 50 eV. Data acquisition and handling were done via the Thermo Avantage software by Parry et al. Spectra were fitted with one or more Voigt profiles and Scofield sensitivity factors were applied for quantification. All spectra were referenced in binding energy to the hydrocarbon C 1s peak at 285 eV. Before XPS measurements, all samples were washed three times with DMC and mounted on a sample holder using conductive copper tape. The sample preparation was carried out in an argon-filled glovebox (H<sub>2</sub>O and O<sub>2</sub> < 1 ppm). The transfer to the spectrometer was done via a transfer module under inert gas conditions. To ensure the stability of the SEI in delithiated states, the electrode potential was held for 10 h after the electrochemical delithiation.

## Supporting Information

Supporting Information is available from the Wiley Online Library or from the author.

## Acknowledgements

This work was financially supported by the China Scholarship Council (no. 201506880038) and contributes to the research conducted at CELEST (Center for Electrochemical Energy Storage Ulm-Karlsruhe). A.B. and A.B. thank the Deutsche Forschungsgemeinschaft (DFG) within the project “EDLstruct” (BA 4956/8-1) for the financial support.

Open access funding enabled and organized by Projekt DEAL.

## Conflict of Interest

The authors declare no conflict of interest.

## Data Availability Statement

The data that support the findings of this study are available from the corresponding author upon reasonable request.

## Keywords

conversion reactions, electrolytes, lithium-ion batteries, organic solvents, solid electrolyte interphases

Received: March 30, 2021

Revised: May 14, 2021

Published online: June 1, 2021

- [1] D. Bresser, S. Passerini, B. Scrosati, *Energy Environ. Sci.* **2016**, *9*, 3348.
- [2] L. Wang, G. Zhang, Q. Liu, H. Duan, *Mater. Chem. Front.* **2018**, *2*, 1414.
- [3] G. Tian, Z. Zhao, A. Sarapulova, C. Das, L. Zhu, S. Liu, A. Missiul, E. Welter, J. Maibach, S. Dsoke, *J. Mater. Chem. A* **2019**, *7*, 15640.
- [4] C. Yuan, H. B. Wu, Y. Xie, X. W. D. Lou, *Angew. Chem., Int. Ed.* **2014**, *53*, 1488.
- [5] S.-W. Kim, H.-W. Lee, P. Muralidharan, D.-H. Seo, W.-S. Yoon, D. K. Kim, K. Kang, *Nano Res.* **2011**, *4*, 505.
- [6] Z. Zhao, G. Tian, A. Sarapulova, V. Trouillet, Q. Fu, U. Geckle, H. Ehrenberg, S. Dsoke, *J. Mater. Chem. A* **2018**, *6*, 19381.
- [7] a) M. Abdollahifar, S.-S. Huang, Y.-H. Lin, Y.-C. Lin, B.-Y. Shih, H.-S. Sheu, Y.-F. Liao, N.-L. Wu, *Journal of Power Sources* **2018**, *378*, 90; b) Z. Zhao, G. Tian, A. Sarapulova, G. Melinte, J. L. Gómez-Urbano, C. Li, S. Liu, E. Welter, M. Etter, S. Dsoke, *ACS Appl. Mater. Interfaces* **2019**, *11*, 29888.
- [8] a) H. Duncan, F. M. Courtel, Y. Abu-Lebdeh, *J. Electrochem. Soc.* **2015**, *162*, A7110; b) S. Laruelle, S. Grugeon, P. Poizot, M. Dollé, L. Dupont, J.-M. Tarascon, *J. Electrochem. Soc.* **2002**, *149*, A627; c) S. J. Rezvani, F. Nobili, R. Gunnella, M. Ali, R. Tossici, S. Passerini, A. Di Cicco, *J. Phys. Chem. C* **2017**, *121*, 26379.
- [9] D. Aurbach, *J. Electrochem. Soc.* **1996**, *143*, 3809.
- [10] D. Aurbach, Y. Talyosef, B. Markovsky, E. Markevich, E. Zinigrad, L. Asraf, J. S. Gnanaraj, H.-J. Kim, *Electrochim. Acta* **2004**, *50*, 247.
- [11] a) E. Peled, S. Menkin, *J. Electrochem. Soc.* **2017**, *164*, A1703; b) P. Verma, P. Maire, P. Novák, *Electrochim. Acta* **2010**, *55*, 6332.
- [12] C. Arbizzani, G. Gabrielli, M. Mastragostino, *J. Power Sources* **2011**, *196*, 4801.
- [13] a) G. Zampardi, F. La Mantia, *Batteries Supercaps* **2020**, *3*, 672; b) X. Wang, E. Yasukawa, S. Mori, *Electrochim. Acta* **2000**, *45*, 2677; c) S.-T. Myung, Y. Hitoshi, Y.-K. Sun, *J. Mater. Chem.* **2011**, *21*, 9891; d) J. Mun, T. Yim, C. Y. Choi, J. H. Ryu, Y. G. Kim, S. M. Oh, *Electrochem. Solid-State Lett.* **2010**, *13*, A109; e) E. Krämer, T. Schedlbauer, B. Hoffmann, L. Terborg, S. Nowak, H. J. Gores, S. Passerini, M. Winter, *J. Electrochem. Soc.* **2013**, *160*, A356; f) A. Heckmann, M. Krott, B. Streipert, S. Uhlenbruck, M. Winter, T. Placke, *Chemphyschem* **2017**, *18*, 156.
- [14] P. Meister, X. Qi, R. Kloepsch, E. Krämer, B. Streipert, M. Winter, T. Placke, *ChemSusChem* **2017**, *10*, 804.
- [15] M. Arnaiz, E. Goikolea, T. Rojo, L. Wittscher, A. Balducci, J. Ajuria, *J. Power Sources* **2019**, *434*, 226757.
- [16] a) S. Brox, S. Röser, T. Husch, S. Hildebrand, O. Fromm, M. Korth, M. Winter, I. Cekic-Laskovic, *ChemSusChem* **2016**, *9*, 1704; b) S. Brox, S. Röser, B. Streipert, S. Hildebrand, U. Rodehorst, X. Qi, R. Wagner, M. Winter, I. Cekic-Laskovic, *ChemElectroChem* **2017**, *4*, 304; c) J. Krummacher, A. Balducci, *Chem. Mater.* **2018**, *30*, 4857;

- d) C. Schütter, S. Passerini, M. Korth, A. Balducci, *Electrochimica Acta* **2017**, 224, 278.
- [17] C. Schütter, T. Husch, V. Viswanathan, S. Passerini, A. Balducci, M. Korth, *J. Power Sources* **2016**, 326, 541.
- [18] a) A. Andersson, A. Henningson, H. Siegbahn, U. Jansson, K. Edström, *J. Power Sources* **2003**, 119–121, 522; b) D. Briggs, D. R. Clarke, S. Suresh, I. M. Ward, M. H. Black, *Surface Analysis of Polymers by XPS and Static SIMS*, Cambridge University Press, Cambridge **2009**; c) F. Jeschull, J. Maibach, R. Félix, M. Wohlfahrt-Mehrens, K. Edström, M. Memm, D. Brandell, *ACS Appl. Energy Mater.* **2018**, 1, 5176; d) S. Leroy, H. Martinez, R. Dedryvère, D. Lemordant, D. Gonbeau, *Appl. Surf. Sci.* **2007**, 253, 4895; e) F. Tao, Z. H. Wang, M. H. Qiao, Q. Liu, W. S. Sim, G. Q. Xu, *J. Chem. Phys.* **2001**, 115, 8563.
- [19] N. Chaix, F. Alloin, J.-P. Bélières, J. Saunier, J.-Y. Sanchez, *Electrochim. Acta* **2002**, 47, 1327.
- [20] L. El Ouatani, R. Dedryvère, C. Siret, P. Biensan, S. Reynaud, P. Iratçabal, D. Gonbeau, *J. Electrochem. Soc.* **2009**, 156, A103.
- [21] a) M. Nie, J. Demeaux, B. T. Young, D. R. Heskett, Y. Chen, A. Bose, J. C. Woicik, B. L. Lucht, *J. Electrochem. Soc.* **2015**, 162, A7008; b) H. Ota, Y. Sakata, A. Inoue, S. Yamaguchi, *J. Electrochem. Soc.* **2004**, 151, A1659.